Structure and Mechanical Properties of Compressed Sodium Aluminosilicate Glasses: Role of Non-Bridging Oxygens

Tobias K. Bechgaard[1], Ashutosh Goel[2], Randall E. Youngman[3], John C. Mauro[3], Sylwester J. Rzoska[4], Michal Bockowski[4], Lars R. Jensen[5], Morten M. Smedskjaer[1,*]

[1] *Department of Chemistry and Bioscience, Aalborg University, Aalborg, Denmark*

[2] *Department of Materials Science and Engineering, Rutgers, The State University of New Jersey, Piscataway, NJ, USA*

[3] *Science and Technology Division, Corning Incorporated, Corning, USA*

[4] *Institute of High-Pressure Physics, Polish Academy of Sciences, Warsaw, Poland*

[5] *Department of Mechanical and Manufacturing Engineering, Aalborg University, Aalborg, Denmark*

* Corresponding author. e-mail: <u>mos@bio.aau.dk</u>

Abstract: Clarifying the effect of pressure on the structure of aluminosilicate glasses is important for understanding the densification mechanism of these materials under pressure and the corresponding changes in macroscopic properties. In this study, we examine changes in density, network structure, indentation hardness, and crack resistance of sodium aluminosilicate glasses with varying Al/Si ratio and thus non-bridging oxygen (NBO) content before and after 1 GPa isostatic compression at elevated temperature. With increasing NBO content, the silicate network depolymerizes, resulting in higher atomic packing density, lower hardness, and higher crack resistance. The ability of the glasses to densify under isostatic compression is higher in the high-NBO glasses and these glasses also exhibit more pronounced pressure-induced changes in mechanical properties. The ^{27}Al NMR data show a surprising presence of five-fold aluminum in the as-made high-NBO glasses, with additional formation upon compression. Our study therefore provides new insights into the complicated relationship between Al coordination and NBO content in aluminosilicate glasses and how it affects their densification behavior.

Keywords: aluminosilicate glass, structure, non-bridging oxygen, pressure, indentation

1. Introduction

The relationship between structure and properties for sodium aluminosilicate ($Na_2O-Al_2O_3-SiO_2$) glasses and glass-forming liquids with varying thermodynamic variables (e.g., composition, temperature, and pressure) are important for both industrial and geological processes. These glasses are commercially used for various products, such as flat panel display glass, scratch resistant cover glass, and nuclear waste glass. The three oxides constitute more than 80% of andesitic and granitic magmatic systems and therefore also have important implications for magma dynamics and properties.

Several structural models have proposed that for Al/Na ratio $\leq$ 1, i.e., excess Na^+ ions, all Al^{3+} is found in tetrahedral configuration (Al^{IV}) [1-4]. Addition of Al_2O_3 to an alkali silicate glass ideally leads to the removal of the network-modifying Na^+ ions from their original role in the network until no more non-bridging oxygen (NBO) atoms remain [5]. For Al/Na ratio $\geq$ 1, some Al^{3+} ions can no longer be charge balanced in tetrahedral configuration and some excess Al^{3+} is forced into higher coordination number (five-fold Al^V or six-fold Al^{VI}) as a means of charge-balancing additional Al tetrahedra [6-8]. An alternative hypothesis is that Al^{IV} can be incorporated, even in peraluminous compositions, without the need for a charge-balancing cation through association with a three-coordinated oxygen (oxygen tricluster) [9-11]. In any case, it is well accepted that a range of macroscopic properties (e.g., transport and mechanical) depend on the Al/Na ratio and thus the network connectivity [12-15], i.e., the fraction of NBOs.

Clarifying the effect of pressure on the structure of aluminosilicate glasses is important for understanding the densification mechanism of these materials under pressure and the corresponding changes in macroscopic properties. However, high-pressure experiments are challenging, partly due to the typical small sample volumes [16], prohibiting characterization of post-compression properties. In this work, we investigate sodium aluminosilicate glasses quenched under isostatic pressure from the glass transition temperature in a nitrogen gas pressure chamber. Although this approach is relatively modest in both temperature and pressure (~T_g and $\leq$1 GPa), it permits permanent densification of relatively large glass pieces (cm^2) that are suitable for characterization of, e.g., mechanical properties

[17,18]. This is because permanent densification of glass occurs at significantly lower pressures for compression at elevated temperature compared to that at room temperature [19,20].

Pressure-induced structural changes of aluminosilicates are manifested by changes in both short- and intermediate-range structure, including increase in the local coordination numbers of the network forming Al and Si cations from 4 to 5 and 6, enabling closer packing of the structural units. This coordination number change has been reported to involve conversion of NBO to bridging oxygen (BO) [21-24], but in the absence of NBOs, it can also occur through the formation of oxygen triclusters [25,26]. The densification mechanism of sodium aluminosilicate has also been suggested to include decrease of Na-O bond distances [23,27,28], decrease of inter-tetrahedral bond angles [29,30], decrease of average ring size [31], and increase in distribution of Si-O and Al-O bond lengths [30].

In this work, we study the structure and micromechanical properties of a series of Na_2O-Al_2O_3-SiO_2 glasses before and after isostatic compression at elevated temperature. Specifically we study the influence of NBOs on the changes in structure and properties by varying the Al/Si ratio at constant Na_2O concentration. Our results provide insight into the composition-dependent structural changes that facilitate densification of the aluminosilicate network during compression and the consequence for the micromechanical properties. Improved understanding of the link among structure and mechanical properties is important due to the need for more scratch-resistant and mechanically durable glasses to enable new advanced glass applications.

2. Experimental Section

2.1 Sample preparation

We have prepared six glasses in the $(75-x)SiO_2$-xAl_2O_3-$25Na_2O$ system with x = 0, 5, 10, 15, 20, and 25. In this series, the $[Al_2O_3]/[Na_2O]$ ratio is ≤ 1 and therefore prevailing models of network structure in peralkaline glasses would indicate sufficient charge-compensating Na^+ ions to keep all Al^{3+} in tetrahedral configuration. High purity powders of SiO_2 (Alfa Aesar; >99.5%), Na_2CO_3 (Sigma Aldrich; >99%), and Al_2O_3 (Sigma Aldrich; ≥99%) were used for glass melting. Homogeneous mixtures of batches (corresponding to ~70 g of oxides), obtained by ball milling, were melted in Pt-

Rh crucibles at 1650 ℃ for 2 h in air. The melts were poured on a metallic table and were initially annealed at 600 ℃ for 1 h. The chemical compositions of the glasses were determined using flame emission spectroscopy and inductively coupled plasma mass spectroscopy. The results are given in Table 1. To ensure uniform thermal history, the glasses were annealed at their respective glass transition temperature (T_g) for ~2 h. T_g was determined using differential scanning calorimetry (DSC 449C, Netzsch) at 10 K/min (Table 1). The glasses were cut to dimensions of about $10 \times 10 \times 8$ mm^3 and polished to an optical finish.

The six glass compositions were isostatically compressed at 0.5 and 1.0 GPa at their respective ambient pressure T_g value (see Table 1) in a gas pressure reactor with nitrogen as the compression medium. The system was kept at the high-pressure/high-temperature condition for 30 min before cooling to room temperature at 60 K/min, followed by decompression at room temperature at 30 MPa/min. The setup used for this pressure treatment has been described in detail in Ref. [17]. X-ray diffraction analyses showed no evidence of crystallization following the pressure treatment.

2.2 Density

The density values of the as-prepared and compressed glass samples were determined using Archimedes' principle with ethanol as the immersion medium. The weight of each glass sample in both air and ethanol was measured ten times.

2.3 Indentation

Vickers hardness (H_V) and crack resistance (CR) of as-prepared and isostatically compressed glasses were measured using a Vickers micro-indenter (Duramin 5, Struers A/S). The measurements were performed in air at room temperature with a dwell time of 15 s. Thirty indentations at each load (0.49, 0.98, 1.96, 2.94, 4.91, 9.81, and 19.6 N) were performed. H_V was calculated at 0.98 N from the length of the indentation diagonals. CR was determined as the load leading to an average of two radial cracks per indent [35].

2.4 Raman Spectroscopy

Raman scattering spectra were measured in backscattering geometry with a Renishaw Invia Raman microscope on freshly polished samples. A diode laser with a wavelength of 532 nm was used as the excitation source. The collected Raman spectra were baseline-corrected using an asymmetric least square algorithm [32]. Afterwards the processed spectra were deconvoluted using Fityk software with Gaussian and Voigt lineshapes.

2.5 ^{27}Al NMR Spectroscopy

^{27}Al magic-angle spinning (MAS) nuclear magnetic resonance (NMR) and triple quantum magic-angle spinning (3QMAS) NMR experiments on both as-prepared and compressed (1.0 GPa) aluminosilicate glasses were conducted at 16.4T using a commercial spectrometer (VNMRs, Agilent) and a 1.6mm MAS NMR probe (Agilent) with spinning speeds of 25 kHz. MAS NMR data were acquired using radio frequency pulses of 0.6 μs (equivalent to a π/12 tip angle), relaxation delays of 2 s, and signal averaging of 1000 acquisitions. MAS NMR data were processed using commercial software, without additional apodization and referenced to aqueous aluminum nitrate at 0.0 ppm. A weak background signal from the zirconia MAS rotors was detected by ^{27}Al MAS NMR of an empty rotor and subsequently subtracted from the MAS NMR data of the glass samples. This signal, at approximately 16 ppm, is clearly distinct from the Al peaks in the glasses, but nonetheless has been removed to ensure higher accuracy in the ^{27}Al MAS NMR experiments. Unfortunately, this weak zirconia signal cannot be removed from ^{27}Al 3QMAS NMR data, and appears in some of the spectra as a weak set of contours around 16 ppm in the MAS NMR dimension.

MQMAS NMR spectra were measured using the three pulse, zero quantum filtering method [33]. The hard 3π/2 and π/2 pulse widths were calibrated to 1.8 and 0.7 μs, and the soft reading pulse of the z-filter was optimized to 10 μs. 48 scans were collected for each of 88 t_1 points, using a recycle delay of 1 s. Spectra were processed using commercial software (VNMRJ, Agilent) and modest line broadening (100 Hz) was used in processing the ^{27}Al 3QMAS NMR data. For each resonance in the 3QMAS NMR spectra, the centers of gravity in the MAS and isotropic dimensions, δ_2^{CG} and δ_{iso}^{CG},

were used to calculate the isotropic chemical shift (δ_{CS}) and the quadrupolar coupling product (P_q) according to

$$\delta_{CS} = \frac{10}{27}\delta_2^{CG} + \frac{17}{27}\delta_{iso}^{CG} \tag{1}$$

and

$$P_q = \left(\delta_{iso}^{CG} - \delta_2^{CG}\right)^{1/2} * f(S) * \nu_0 * 10^{-3}, \tag{2}$$

where $f(S)$ = 10.244 for spin-5/2 nuclei (^{27}Al), and ν_0 is the resonance frequency of the quadrupolar nucleus in MHz [34]. P_q from Eq. (2) can be related to the quadrupolar coupling constant (C_q) as $P_q = C_q(1+\eta_q^2/3)^{1/2}$, where η_q is the quadrupolar coupling asymmetry parameter. P_q and C_q are often used interchangeably, with small errors introduced when neglecting the contribution of η_q.

3. Results and Discussion

3.1 Glass Transition Temperature and Density

As given in Table 1, T_g increases with increasing Al_2O_3/Na_2O ratio. This is because the number of non-bridging oxygens per tetrahedrally coordinated cation (NBO/T) decreases with increasing Al_2O_3/Na_2O ratio, i.e., the network connectivity increases. Values of NBO/T are also given in Table 1, which have been calculated from the analyzed compositions by assuming that all available Na^+ ions are used for charge-balancing Al tetrahedra and by neglecting the presence of oxygen triclusters and free oxide. The compositional variation of density is shown in Fig. 1a. Density increases with increasing Al_2O_3 content throughout the studied peralkaline composition space. The measured values of T_g and densities are generally in agreement with those reported previously [1,36]

For all glass compositions, the density increases approximately linearly with the applied pressure (Fig. 1a). Since the Al_2O_3-for-SiO_2 substitution changes the average molar mass of the glasses, we calculated the atomic packing factor (APF) of the glasses to evaluate differences in free volume. APF is the ratio between the minimum theoretical volume occupied by the ions (assumed to be spherical) and the corresponding molar volume of the glass. The assumed coordination numbers (2 for O, 4 for Si and Al^{IV}, 5 for Al^{V}, and 6 for Na) along with the corresponding effective ionic radii of Shannon

[37] have been used to calculate the minimum theoretical volume occupied by the ions. We note that the average coordination number of Na in peralkaline aluminosilicate glasses is in the range 6-8 [38-40], which would change the absolute values of APF by maximum 1-2%. The molar volume is calculated as the ratio between the molar mass and measured density from Table 1. We find that SiO_2-rich glasses have a larger atomic packing factor and thus smaller free volume than the Al_2O_3-rich compositions (Fig. 1b).

Based on the linear relation between density and applied pressure for each glass (Fig. 1a), we calculate the irreversible plastic compressibility, which is defined as $-(1/V)(dV/dp)$. This is the volume change measured after decompression to ambient pressure. We find that the plastic compressibility is larger in the SiO_2-rich glasses (Table 1). This is not in agreement with the observed trend in compressibility, since the glasses with smaller free volume are more prone to network compaction upon pressure treatment at elevated temperature. Instead, it appears that the plastic compressibility of the glasses is positively correlated to NBO/T as shown in Fig. 1c. That is, flexible glasses containing NBOs exhibit a larger capability to undergo densification.

3.2 Hardness and Crack Resistance

Vickers hardness has been determined by micro-indentation at 9.81 N and is a measure of the ability of the glasses to resist elastoplastic deformation. Hardness increases with increasing Al/Na ratio and then appears to saturate around $[Al_2O_3]=[Na_2O]=25$ mol% (Fig. 2). This composition dependence is likely caused by the reduction in the number of NBOs with increasing Al/Na ratio [36]. The reduction in the number of NBOs increases the rigidity of the network [41], which in turn decreases the ability of the glass to deform. Isostatic compression increases the hardness of all compositions (Fig. 2). The pressure-induced increase in hardness has been shown to be related to the ability of the glass to deform under the indentation tip. The glass volume available for densification beneath the indentation tip in the as-prepared glass is larger than that in the corresponding isostatically compressed glass, resulting in a larger resistance to densification and an increase in hardness [42]. As shown in the inset of Fig. 2, we find an apparent positive relation between the slope of the hardness vs pressure (dH_V/dp)

7

and the plastic compressibility, suggesting that the overall network densification is responsible for the increase in hardness upon compression.

Crack initiation occurs at sufficiently high loads in a Vickers indentation test and has been attributed to the mismatch between the plastically deformed volume and the surrounding elastically deformed matter [43-45]. The crack resistance (CR) is derived as the load at which an average of two radial cracks form. CR decreases with increasing Al/Na ratio (Fig. 3), presumably due to a decrease in the densification ability of glass as NBOs are removed from the network. A glass which can be easily densified allows for decrease in the residual stress around the indent, which results in an increase in crack resistance [46]. Hence, the decrease in densification ability as the glass becomes more rigid decreases its crack resistance. The pressure-induced decrease in crack resistance is related to the densification of the glass during hot isostatic compression, which decreases the ability of the glass to deform further during subsequent indentation. The decrease in densification degree following isostatic compression increases the residual stress around the indent, which results in a decrease in crack resistance [42,46].

3.3 Raman Spectroscopy

Raman spectroscopy has been used to study the structural differences in the glass series due to differences in their composition and pressure history. The Raman spectra are all collected on glasses at ambient conditions and can be divided into three regions: low frequency region (250-700 cm^{-1}), intermediate frequency region (700-870 cm^{-1}), and high frequency region (870-1300 cm^{-1}). We note that when interpreting Raman spectra, it is not possible to distinguish between Al and Si based tetrahedra [38]. Q^n will refer to tetrahedrally coordinated Si^{4+} or Al^{3+} with n bridging oxygens and 4-n non-bridging oxygens. In general, our observations are in agreement with previous Raman results on related sodium aluminosilicate glasses [47-50].

First we consider the annealed glasses prior to isostatic compression (Fig. 4). In the low frequency region, two distinct bands are observed. The Raman shift and intensity of these signals depend on the Al/Na ratio. In the Al_2O_3-free glass (Al-0), they are located at ~540 cm^{-1} with a shoulder at ~600 cm^{-1}, corresponding to Q^3 units and three-membered tetrahedral rings in the glass,

respectively [38]. When the Al_2O_3 content increases, the Raman shifts of the two bands decrease, approaching ~490 and ~560 cm^{-1}, respectively, in the Al-25 glass, which is illustrated in Fig. 5 for the band at ~500 cm^{-1}. For the Al_2O_3-containing glasses, the band at ~500 cm^{-1} likely corresponds to Q^4 units [50]. For Al-5, the higher frequency band is split into two peaks at ~580 and ~590 cm^{-1}, corresponding to three-membered rings containing one or more Al atoms and pure SiO_4 three-membered rings, respectively [48]. The existence of two distinct signals is explained by the substitution of Al_2O_3 into the glass, decreasing the bond strength in the Al-containing tetrahedral rings and therefore shifting the signal towards lower frequencies [38]. Furthermore, the intensity of the lower frequency band at ~540 cm^{-1} in the Al_2O_3-free glass indicates that a significant proportion of Q^3 units are present in the glass, whereas the intensity of the band at ~500 cm^{-1} in the Al_2O_3-containing glasses indicates the presence of an increasing proportion of Q^4 units with increasing Al_2O_3 content [38]. The long tail at lower frequencies (~250 to ~450 cm^{-1}), which is observed in all glasses (Fig. 4), is caused by the stretching of O atoms in large tetrahedral rings with five or more members [38].

In the intermediate frequency region, one broad band can be found. The contributions to the band in this region are strongly convoluted and poorly known [51], but we note that the peak position systematically shift towards lower frequencies when substituting Al_2O_3 for SiO_2 (Fig. 5). This is explained by a decrease in bond strength due to a decrease in the force constant as SiO_2 and Al_2O_3 mix [52]. In the high frequency region, two bands are visible in the Raman spectra of the low-Al_2O_3 glasses (Al-0 to Al-15), while only one band is evident in the high-Al_2O_3 glasses (Al-20 and Al-25) due to peak broadening and change of peak position. The position of these bands depend on the Al/Na ratio, i.e., for Al-0 the signals appear around 950 and 1100 cm^{-1} and then at lower frequencies as the Al_2O_3 content increases. These broad bands have been attributed to stretching vibrations of T-O bonds (T = Si, Al) [53,54] and different peaks are convoluted in them. Previously three to five Gaussian peaks have been used for fitting and deconvolution [55,56]. Such spectral deconvolution can reveal quantitative changes in the Q-speciation of the tetrahedral units, i.e., changes in connectivity as a function of the Al/Na ratio. An example of deconvolution of the high frequency band is shown in Fig. 6a for the Al-10 glass. The Gaussian peaks are Q^2 (~950 cm^{-1}), Q^3 (~1050 cm^{-1}), $Q^{4,I}$ (~1125 cm^{-1}), $Q^{4,II}$ (~1100 cm^{-1}), and Q^n (~1000 cm^{-1}) units, which originate from Si-O$^-$ in Q^2 units [38], Si-O$^-$ in Q^3

9

units [38], two Q^4 units with two different local environments [38], and TO$_4$ tetrahedra [48], respectively. The Q^2 and Q^3 peaks are not used to fit the spectrum for Al-25 since no NBOs are expected in this glass composition.

We note that the deconvolution does not give "true" concentrations as the intensity does not only depend on the concentration of the specific structural unit, but also on the local environment, such as next-nearest neighbors and number of NBOs etc. Instead, spectral fitting can be used to qualitatively describe variations in relative proportions of different structural units [51]. The relative areas of the Gaussian peaks used for the deconvolution of these high-frequency bands are shown in Fig. 6b, which reveals an increase in network connectivity with increasing Al/Na ratio. This is comparable to a recent study of compositionally similar glasses [38]. With the addition of alumina, the relative concentration of $Q^{4,II}$ increases at the expense of species with NBOs, i.e., Q^2 and Q^3, since Na$^+$ is used for charge-compensation of Al^{3+} in tetrahedral configuration rather than depolymerization of the network. This is coherent with the general structural model of modified aluminosilicate glasses and the changes in the Raman bands at 490 and 540 cm^{-1} as described above. The deconvolutions suggest that Al^{3+} will preferably enter the network as smaller-angle $Q^{4,II}$ units rather than larger-angle $Q^{4,I}$ units. This preference is explained by the smaller Al-O-Si tetrahedral angles relative to the Si-O-Si tetrahedral angles [38].

Compression of bulk glasses at elevated temperature has been shown to be associated with changes in short- and intermediate-range glass structure [57-60]. Pressure-induced changes in the Raman spectra of aluminosilicate glasses have been found to involve decrease in the relative intensity of the low-frequency region compared to the high-frequency region and changes in the relative intensity of different peaks in the low-frequency region [26]. This effect has been attributed to a suppression of vibrational motion, either by the formation of triclusters, or by a development of bonding character between modifiers and BOs, both of which would inhibit vibrational motions of BOs resulting in a decrease in intensity [26]. Comparison of the acquired Raman spectra of all the as-prepared and compressed glasses in the present study generally does not reveal such decrease in intensity of the low-frequency region relative to the high-frequency region. We have illustrated this in

10

Fig. 7 for the Al-5 glass, which exhibits the largest increase in density and hardness. Instead we next consider ^{27}Al NMR spectroscopy to study the pressure-induced structural changes.

3.4 ^{27}Al NMR Spectroscopy

Figure 8a shows ^{27}Al MAS NMR spectra of the as-prepared aluminosilicate glasses. These spectra are characterized by an intense peak centered around 60 ppm, which moves to higher frequencies with increasing Al_2O_3 content. This resonance corresponds to four-fold coordinated aluminum (Al^{IV}), and the change in MAS NMR shift with Al_2O_3 content is consistent with the changes in next-nearest neighbor cations (Si or Al). The Al-5 glass, with smallest MAS NMR shift, has Al^{IV} surrounded by silicon, while the high Al_2O_3 glasses, with MAS NMR shifts approaching 62 ppm, have more instances where aluminum has replaced silicon as a next-nearest neighbor cation [61]. This is consistent with mixing of the Al and Si tetrahedra in these networks, as demonstrated by the Raman spectroscopy results discussed above.

In addition to Al^{IV} groups, there is some evidence for higher coordination sites (Al^V) in some of these as-prepared glasses. The two compositions with lowest Al_2O_3 content, Al-5 and Al-10, exhibit an additional MAS NMR signal around 20 ppm, as shown in the inset to Figure 8a. This resonance is consistent with Al^V groups, which are unexpected for these highly peralkaline glasses. Furthermore, this Al^V resonance near 20 ppm is decreasing in intensity with increasing Al_2O_3 content, and is completely absent for the Al-25 glass, which is the only glass with $Al_2O_3=Na_2O$. This behavior in Al^V concentration with glass composition is rather unusual given the prevailing models for Al^{IV} compensation in peralkaline aluminosilicate glasses. However, there have been a couple of related studies showing non-zero Al^V concentrations in highly peralkaline glasses, including the sodium aluminosilicate system [62]. This work by Malfait and co-workers suggested that the exchange between NBO and Al^V groups was at least partially responsible for the presence of Al^V in peralkaline compositions. In the case of Al-5 and Al-10 glasses in the present work, the NBO content is quite high (Table 1) and it is possible that more Al^V polyhedra can be energetically stabilized in such glasses. The presence of higher coordinated Al in the most peralkaline glasses is also consistent with

an unexpected observation of Ga^{VI} groups in chalcogenide glasses having sufficient phosphorus content to fully stabilize Ga in tetrahedral coordination [63].

A better understanding of the Al environments in these glasses is achieved through analysis of the ^{27}Al 3QMAS NMR spectra, where the positions in both MAS and isotropic dimensions are used to separate isotropic chemical shifts from quadrupolar coupling induced shifts, both of which contribute to the MAS NMR shifts in Figure 8a. These data also provide enhanced spectral resolution and are often used to identify aluminum sites with different coordination numbers [64]. The two-dimensional contour plot in Figure 8b, for the as-prepared Al-5 glass, shows two distinct resonances, assigned to Al^{IV} and Al^{V} groups, confirming the peak assignments in the corresponding MAS NMR data. The 3QMAS NMR spectra for these glasses also indicate that octahedral Al (Al^{VI} groups) do not appear to be present in any of the as-made glasses. This means that the extra intensity in the inset to Figure 8a, attributed to Al^{V}, does indeed belong only to Al^{V} groups, with little to no contribution from Al^{VI}. δ_{CS} and P_q, the calculations of which are described in Section 2.5, are given in Table 2 for all of the as-prepared glasses. The trend in δ_{CS}, which accounts for the changing MAS NMR shifts of Figure 8a, confirms an increase in chemical shielding of 4 ppm between the low and high Al_2O_3 glasses. Such changes in Al^{IV} environment are consistent with a gradual change in the local configuration of these tetrahedral network elements, especially in the identity of next-nearest neighbor cations. Previous NMR studies of glasses in the sodium aluminosilicate ternary indicate essentially no change in the chemical shift of Al^{IV} groups as Al_2O_3 content is increased [38]. Their interpretation was for Al^{IV} groups being surrounded entirely by silica tetrahedra, regardless of the glass composition and consistent with the Lowenstein rule of aluminum avoidance (i.e., no Al-O-Al connectivity) [65]. However, the data in Figure 8a and Table 2 clearly indicate that the Al^{IV} groups are progressively deshielded with increasing $[Al_2O_3]$ in the current study, suggesting some violation of the aluminum avoidance. In addition to changes in isotropic chemical shift, the Al^{IV} groups in these glasses also are characterized by a progressively larger P_q (Table 2), pointing towards higher distortion of the tetrahedral units with increasing Al_2O_3. This has been associated with changing Al-O bond distances

or possibly a change in interaction between the Al^{IV} tetrahedra and charge-compensating sodium cations [38].

Compressed analogues to these sodium aluminosilicate glasses have also been examined with ^{27}Al MAS and 3QMAS NMR spectroscopy. The ^{27}Al MAS NMR spectra for the five compressed glasses are plotted in Figure 9a, showing that most aluminum remains in Al^{IV} polyhedra upon compression, but given the more apparent Al^{V} signal around 30 ppm, also shows that some aluminum has been forced into Al^{V} groups with compression. The increased intensity of the Al^{V} peak is also evident in ^{27}Al 3QMAS NMR spectra of these compressed glasses, as shown by the contour plot for Al-5 in Figure 9b. The contours for Al^{V} are indeed more intense after compression of the glass. Full analysis of δ_{CS} and P_q for the compressed glasses are given in Table 2. The Al^{IV} groups in the compressed glasses exhibit nearly identical chemical shifts as in their as-made counterparts, indicating the close similarity in structural environment for Al^{IV} polyhedra before and after compression. In other words, compression does not appear to lead to any change in how Al^{IV} groups are connected into the glass network (e.g., Al-O-Si and Al-O-Al bonding). However, there are distinct changes in P_q with compression, where for all glass compositions, the P_q values increase with this treatment. This does indicate that the symmetry around Al^{IV} polyhedra is impacted by pressure, and the larger magnitude of the quadrupolar coupling parameter suggests more distortion after compression. Changes in Al^{V} parameters, both δ_{CS} and P_q, are less systematic with composition and in fact are probably insignificant given the low abundance of Al^{V} and correspondingly low signal-to-noise ratio in the NMR data. δ_{CS} is around 30 ppm for Al^{V} in both as-made and compressed glasses, consistent with other studies of Al^{V} in aluminosilicates [49,66]. Likewise, the P_q values around 5 MHz are also similar between as-made and compressed glasses.

The largest change in aluminum speciation due to glass compression is a change in Al^{IV} and Al^{V} site populations. The ^{27}Al NMR spectra in Figures 8 and 9 indicate an increase in Al^{V} concentration with compression, which is quite apparent when comparing the isotropic projections from ^{27}Al 3QMAS NMR (Figure 10). Here, isotropic data from the 3QMAS NMR experiments are overlaid for each glass composition, showing an increase in Al^{V} content for the two glasses with these polyhedra

in their as-made forms (Al-5 and Al-10), as well as the appearance of Al^V in the Al-15 glass only after compression. All other compressed glasses do not exhibit Al^V resonances in their ^{27}Al MAS and 3QMAS NMR data, and thus the concentration of Al^V in these glasses is negligible. As shown by the comparisons in Figure 10, aluminum coordination is sensitive to compression, similar to previous work on commercial aluminosilicates [18], and also the fictive temperature dependence of Al speciation in aluminosilicates [67]. The main change in Al coordination number occurs in glasses which already contained a non-zero Al^V population and high NBO content in their pre-compressed states (Figure 11). Al-5 shows an increase of approximately 2.5%, compared to 1% and 0.3% in the Al-10 and Al-15 glasses, respectively (Table 2).

The effects of NBOs and compression on the generation of Al^V is shown in Figure 11, where NBOs and pressure is positively correlated to the presence of Al^V. In agreement with our result, a larger pressure-induced generation of Al^V in aluminosilicate glasses with NBOs has previously been reported in literature [68-70]. For such glasses, the simple proposed mechanism in the studied pressure range is $Al^{IV} + NBO \leftrightarrow Al^V$. This mechanism has been directly supported by changes in the oxygen speciation as probed by ^{17}O 3Q MAS NMR spectroscopy [68]. Although not observed herein at 1 GPa, pressure-induced formation of Al^V has also been reported in sodium aluminosilicate glasses with little or no NBO (e.g., albite $NaAlSi_3O_8$) [70,71], suggesting that alternative mechanisms could also be at play at higher pressure ranges, e.g., when most of the NBOs have already been consumed in increasing the aluminium coordination number. For example, this could involve formation of NBO and oxygen triclusters and subsequent consumption of NBO to form Al^V [10,64,70], or transformation of a BO to be coordinated with Al^V through formation of oxygen tricluster [70,71]. Finally, we note that in addition to changes in Al^V concentration, the most peralkaline glass (Al-5) also shows a small, but detectable amount of Al^{VI}, but only after compression (Figure 8). This is the only glass, both as-made or compressed, showing any evidence for 6-fold coordinated Al, presumably because Al^{VI} could be formed by a similar mechanism to that of Al^V, i.e., $Al^{IV} + 2NBO \leftrightarrow Al^{VI}$.

4. Conclusion

We have investigated the effect of 1 GPa compression at elevated temperature on structure and mechanical properties of aluminosilicate glasses with varying Al/Si ratio and thus non-bridging oxygen content. Raman and ^{27}Al NMR spectroscopy, density, and Vickers indentation measurements have been performed. We find that the plastic compressibility (i.e., extent of permanent densification) is positively correlated to the number of non-bonding oxygens per tetrahedral (NBO/T), i.e., the network flexibility. Hardness increases while the resistance to initiate radial/median cracks decreases with decreasing NBO/T in the as-made glasses. Upon compression, hardness increases and crack resistance decreases as the ability of the glass to deform decreases upon compression and larger changes in these mechanical properties are found in the high-NBO compositions, consistent with the higher plastic compressibility of these glasses. The Raman spectroscopy measurements on the as-made glasses confirm the expected changes in Q speciation with Na/Al ratio, whereas no major pressure-induced structural changes are evident from the Raman spectra. The ^{27}Al NMR and Raman data both confirm the mixing of the aluminosilicate network, especially as evidenced by the change in chemical shift for the Al^{IV} resonance. Surprisingly, we find the presence of Al^{V} in the as-made glasses, especially when these polyhedra are present only in the most peralkaline glass compositions. Moreover, there is a larger pressure-induced generation of Al^{V}, and in one case Al^{VI}, in aluminosilicate glasses with NBOs. Their presence not only shows a more complicated relationship between Al coordination and NBO content, but also plays a substantial role in the compressibility of these glasses.

References

1. D. E. Day, G. E. Rindone, J. Am. Ceram. Soc. 45 (1962) 579-581.

2. M. Taylor, G. E. Brown., Geochim. Cosmochim. Acta 43 (1979) 1467-1473.

3. P. McMillan, B. Piriou, A. Navrotsky, Geochim. Cosmochim. Acta 46 (1982) 2021-2037.

4. D. A. McKeown, F. L. Galeener, G. E. Brown, J. Non-Cryst. Solids 68 (1984) 361-378.

5. F. Seifert, B. O. Mysen, D. Virgo, Am. Mineral. 67 (1982) 696-717.

6. E. F. Riebling, J. Chem. Phys. 44 (1966) 2857-2865.

7. S. H. Risbud, R. J. Kirkpatrick, A. P. Taglialavore, B. Montez, J. Am. Ceram. Soc. 70 (1987) C10-C12.

8. M. J. Toplis, S. C. Kohn, M. E. Smith, I. J. F. Poplett, Am. Mineral. 85 (2000) 1556-1560.

9. E. D. Lacy, Phys. Chem. Glasses 4 (1963) 234-238.

10. M. J. Toplis, D. B. Dingwell, T. Lenci, Geochim. Cosmochim. Acta 61 (1997) 2605-2612.

11. D. Iuga, C. Morias, Z. Gan, D. R. Neuville, L. Cormier, D. Massiot, J. Am. Chem. Soc. 127 (2005) 11540-11541.

12. D. E. Day, G. E. Rindone, J. Am. Ceram. Soc. 45 (1962) 489-496.

13. T. D. Taylor, G. E. Rindone, J. Am. Ceram. Soc. 53 (1970) 692-695.

14. J. E. Shelby, R. J. Eagan, J. Am. Ceram. Soc. 59 (1976) 420-425.

15. M. M. Smedskjaer, R. E. Youngman, J. C. Mauro, J. Non-Cryst. Solids 381 (2013) 58-64.

16. P. S. Salmon, A. Zeidler, J. Phys.: Condens. Matter 27 (2015) 133201.

17. M. M. Smedskjaer, S. J. Rzoska, M. Bockowski, J. C. Mauro, J. Chem. Phys. 140 (2014) 054511.

18. M. N. Svenson, L. M. Thirion, R. E. Youngman, J. C. Mauro, S. J. Rzoska, M. Bockowski, M. M. Smedskjaer, ACS Appl. Mater. Interfaces 6 (2014) 10436-10444.

19. D. R. Uhlmann, J. Non-Cryst. Solids 13 (1973) 89-99.

20. A. Yamada, S. J. Gaudio, C. E. Lesher, J. Phys.: Conf. Ser. 215 (2010) 012085.

21. J. L. Yarger, K. H. Smith, R. A. Nieman, J. Diefenbacher, G. H. Wolf, B. T. Poe, P. F. McMillan, Science 270 (1995) 1964-1967.

22. S. K. Lee, G. D. Cody, Y. W. Fei, B. O. Mysen, Geochim. Cosmochim. Acta 68 (2004) 4189-4200.

23. S. K. Lee, G. D. Cody, Y. Fei, B. O. Mysen, Chem. Geol. 229 (2006) 162-172.

24. J. R. Allwardt, J. F. Stebbins, B. C. Schmidt, D. J. Frost, A. C. Withers, M. M. Hirschmann, Am. Mineral. 90 (2005) 1218-1222.

25. G. H. Wolf, D. J. Durben, P. F. McMillan, J. Chem. Phys. 93 (1990) 2280-2288.

26. B. T. Poe, C. Romano, N. Zotov, G. Cibin, A. Marcellli, Chem. Geol. 174 (2001) 21-31.

27. N. Shimizu, I. Kushiro, Geochim. Cosmochim. Acta 48 (1984) 1295-1303.

28. S. J. Gaudio, T. G. Edwards, S. Sen, Am. Mineral. 100 (2015) 326-329.

29. D. Sykes, B. T. Poe, P. F. McMillan, R. W. Luth, R. K Sato, Geochim. Cosmochim. Acta 57 (1993) 1753-1759.

30. J. F. Stebbins, D. Sykes, Am. Mineral. 75 (1990) 943-946.

31. M. F. Hochella, G. E. Brown, Geochim. Cosmochim. Acta 49 (1985) 1137-1142.

32. P. H. Eilers, H. F. M. Boelens, Leiden University Medical Centre (2005).

33. J. P. Amoureux, C. Fernandez, S. Steuernagel, J. Magn. Reson. Ser. A 123 (1996) 116.

34. J. P. Amoureux, C. Huguenard, F. Engelke, F. Taulelle, Chem. Phys. Lett. 356 (2003) 497

35. M. Wada, H. Furukawa, K. Fujita, Cer. Soc. Japan 11 (1974) 39.

36. J. E. Shelby, J. Applied Phys. 49 (1978) 5885-5891.

37. R. D. Shannon, Acta Crystallographica Section A 32 (1976) 751-767.

38. D A. McKeown, G. A. Waychunas, G. E. Brown, J. Non-Cryst. Solids 74 (1985) 325-348.

39. X. Xue, J. F. Stebbins, Phys. Chem. Miner. 20 (1993) 297-307.

40. A. M. George, J. F. Stebbins, Phys. Chem. Miner. 23 (1996) 526-534.

41. M. M. Smedskjaer, J. C. Mauro, Y. Yue, Phys. Rev. Letters 105 (2010) 115503.

42. Y. Kato, Yoshinari, H. Yamazaki, S. Yoshida, J. Matsuoka, J. Non-Cryst. Solids 356 (2010) 1768.

43. R. Limbach, A. Winterstein-Beckmann, J. Dellith, D. Möncke, L. Wondraczek, J. Non-Cryst. Solids 417 (2015) 15-27.

44. R. F. Cook, G. M Pharr, J. Am. Cer. Soc. 73 (1990) 787-817.

45. Z. Zhang, N. Soga, K. Hirao, J. Mater. Sci. 30 (1995) 6359-6362.

46. K. G. Aakermann, K. Januchta, J. A. Pedersen, M. N. Svenson, S. J. Rzoska, M. Bockowski, J. C. Mauro, M. Guerette, L. Huang, M. M. Smedskjaer, J. Non-Cryst. Solids 426 (2015) 175-183.

47. C. Le Losq, D. R. Neuville, P. Florian, G. S. Henderson, D. Massiot, Geochim. Cosmochim. Acta 126 (2014) 495-517

48. F. A Seifert, B. O. Mysen, D. Virgo, Am. Mineral. 67 (1982) 696-717

49. D. R Neuville, B.O. Mysen, Geochim. Cosmochim. Acta (1996) 1727-1737.

50. P. McMillan, B. Piriou, J. Non-Cryst. Solids 53 (1982) 279-298.

51. B. O. Mysen, A. Lucier, G. D. Cody, Am. Mineral. 88 (2003) 1668-1678.

52. C. Le Losq, D. R. Neuville, Chem. Geol. 346 (2013) 57-71.

53. R. J. Bell, N. F. Bird, P. Dean, J. Phys. C 1 (1968) 299–303.

54. P. N. Sen, M. F. Thorpe, Phys. Rev. B 15 (1977) 4030–4038.

55. P. F. McMillan Am. Mineral. 69 (1984) 622–644.

56. B. O. Mysen, Eur. J. Mineral. 15 (2003) 781–802.

57. M. M. Smedskjaer, R. E. Youngman, S. Striepe, M. Potuzak, U. Bauer, J. Deubener, H. Behrens, J. C. Mauro, and Y. Yue, Sci. Rep. 4 (2014).

58. M. N. Svenson, T. K. Bechgaard, S. D. Fuglsang, R. H. Pedersen, A. Ø. Tjell, M. B. Østergaard, R. E. Youngman, J. C. Mauro, S. J. Rzoska, M. Bockowski, M. M. Smedskjaer, Phys. Rev. Appl. 2 (2014) 024006.

59. M. B. Østergaard, R. E. Youngman, M. N. Svenson, S. J. Rzoska, M. Bockowski, L. R. Jensen, M. M. Smedskjaer RSC Adv. 5 (2015) 78845-78851.

60. J. Wu, J. Deubener, J.F. Stebbins, L. Grygarova, H. Behrens, L. Wondraczek, Y. Yue, J. Chem. Phys. 131 (2009) 104504.

61. D. R. Neuville, L. Cormier, V. Montouillout, D. Massiot, J. Non-Cryst. Solids 353 (2007) 180-184.

62. W. J. Malfait, R. Verel, P. Ardia, C. Sanchez-Valle, Geochim. Cosmochim. Acta. 77 (2012) 11-26.

63. R. E. Youngman, B. G. Aitken, J. Non-Cryst. Solids. 345 (2004) 50-55.

64. M. E. Smith, K. J. D. Mackenzie. Multinuclear Solid State NMR of Inorganic Materials. Pergamon Materials Series (2002).

65. W. Loewenstein, Am. Mineral. 39 (1954) 92-96.

66. D.R. Neuville, L. Cormier, D. Massiot, Chem. Geol. 229 (2006) 173-185.

67. L. M. Thompson, J. F. Stebbins, Am. Mineral. 98 (2013) 1980-1987.

68. S. K. Lee, G. D. Cody, Y. Fei, B. O. Mysen, Geochim. Cosmochim. Acta 68 (2004) 4189.

69. J. R. Allwardt, J. F. Stebbins, H. Terasaki, L. S. Du, D. J. Frost, A.C . Withers, M. M. Hirschmann, A. Suzuki, E. Ohtani, Am. Mineral. 92 (2007) 1093.

70. S. K. Lee, J. Phys. Chem. B 108 (2004) 5889-5900.

71. S. J. Gaudio, C. E. Lesher, H. Maekawa, S. Sen, Geochim. Cosmochim. Acta 157 (2015) 28.

Table 1. Analyzed chemical compositions (in mol%), calculated number of non-bridging oxygens per tetrahedrally coordinated cation (NBO/T), density (ρ), glass transition temperature (T_g), and plastic compressibility (β). Compositions are analyzed using inductively coupled plasma and flame emission spectroscopy, density determined using Archimedes method, T_g determined using differential scanning calorimetry at a rate of 10 K/min, and β calculated from the slopes of the linear fits to density vs. pressure for each composition.

| Glass ID | Composition (mol%) | | | NBO/T | ρ | T_g | β |
	SiO_2	Al_2O_3	Na_2O	(-)	(g cm^{-3})	(°C)	(GPa^{-1})
Al-0	74.7	0.0	25.3	0.677	2.437	470	0.0215
Al-5	70.0	5.1	24.9	0.494	2.456	500	0.0220
Al-10	64.8	10.2	25.0	0.347	2.471	534	0.0221
Al-15	59.6	15.1	25.3	0.227	2.484	595	0.0187
Al-20	54.6	19.7	25.7	0.128	2.494	638	0.0147
Al-25	49.7	25.2	25.1	0.000	2.498	797	0.0157

Table 2. ^{27}Al NMR parameters determined from 3QMAS NMR spectroscopy. Uncertainties in δ_{CS}, P_q and Intensity are on the order of $\pm$ 0.2 ppm, $\pm$ 0.2 MHz and $\pm$ 0.5%, respectively.

Glass	Al^{IV}			Al^{V}			Al^{VI}		
	δ_{CS} (ppm)	P_q (MHz)	Int (%)	δ_{CS} (ppm)	P_q (MHz)	Int (%)	δ_{CS} (ppm)	P_q (MHz)	Int (%)
Al-5	62.8	4.42	99.4	29.9	4.69	0.6			
Al-5, 1 GPa	62.8	4.69	97.0	29.3	4.98	3.0	-1	4.6	---
Al-10	63.6	4.54	99.7	31	5.28	0.3			
Al-10, 1 GPa	63.8	4.69	98.8	29.7	5.15	1.2			
Al-15	64.3	4.76							
Al-15, 1 GPa	64.5	4.83	99.7	29.6	4.73	0.3			
Al-20	65.3	5.01							
Al-20, 1 GPa	65.6	5.28							
Al-25	66.8	5.82							
Al-25, 1 GPa	67.0	5.94							

Figure 1. (a) Density ρ and (b) atomic packing factor APF of the as-prepared and compressed sodium aluminosilicate glasses as a function of the Al_2O_3 content. Errors associated with the ρ and APF results are smaller than the size of the symbols. APF is calculated as the ratio between the minimum theoretical volume occupied by the ions and the corresponding molar volume of the glass. (c) Plastic compressibility as a function of the calculated number of non-bridging oxygens per tetrahedrally coordinated cation NBO/T. Plastic compressibility is calculated from the slopes of the linear fits to density vs. pressure for each composition.
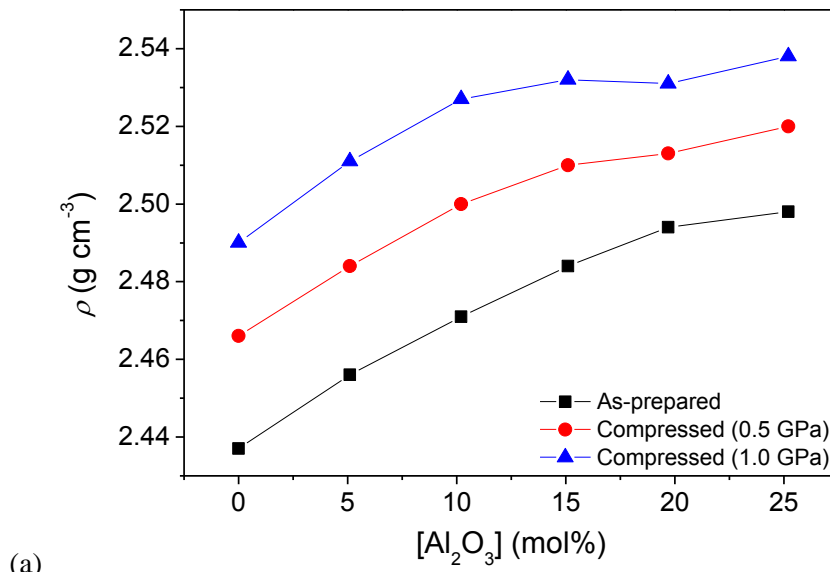
(a)
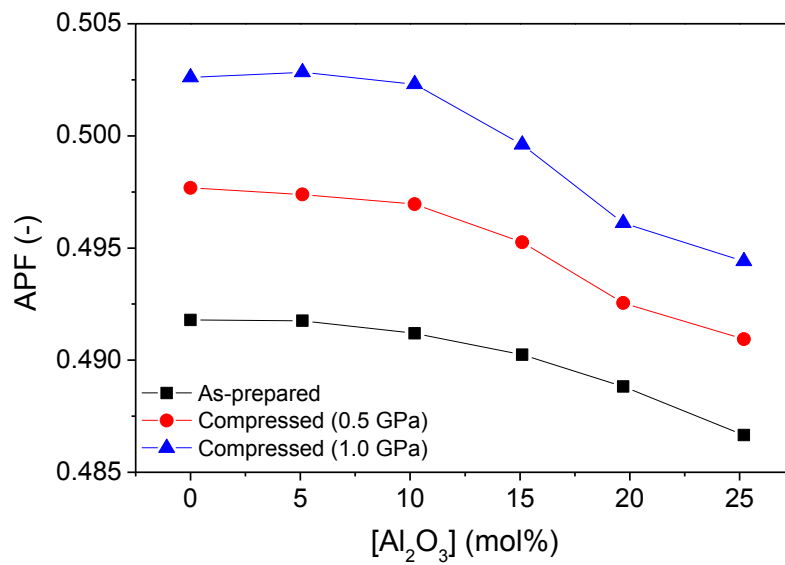
(b)

(Figure 1 continued)
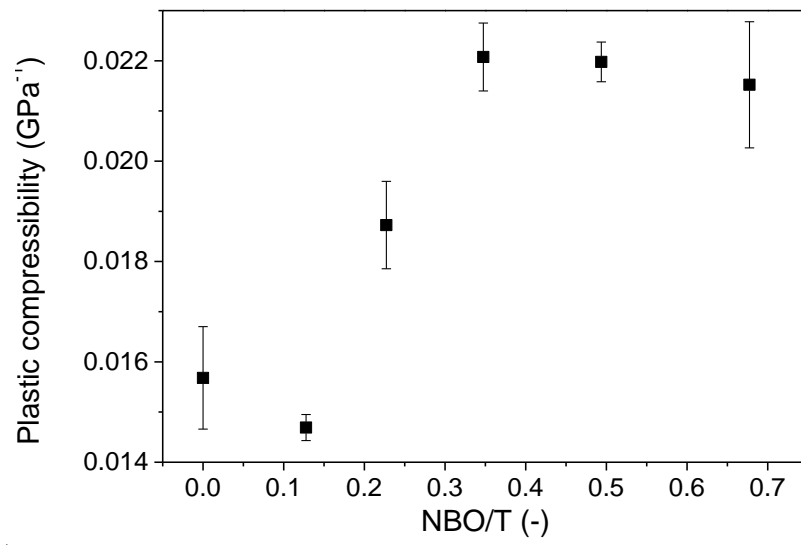
(c)

Figure 2. Vickers hardness (H_V) of the as-prepared and compressed sodium aluminosilicate glasses as a function of the Al_2O_3 content. H_V was measured at an indentation load of 0.98 N. Inset: dependence of the slopes of the hardness vs. pressure curves (dH_V/dp) on the plastic compressibility for the six glasses. The dashed line is a guide for the eye.
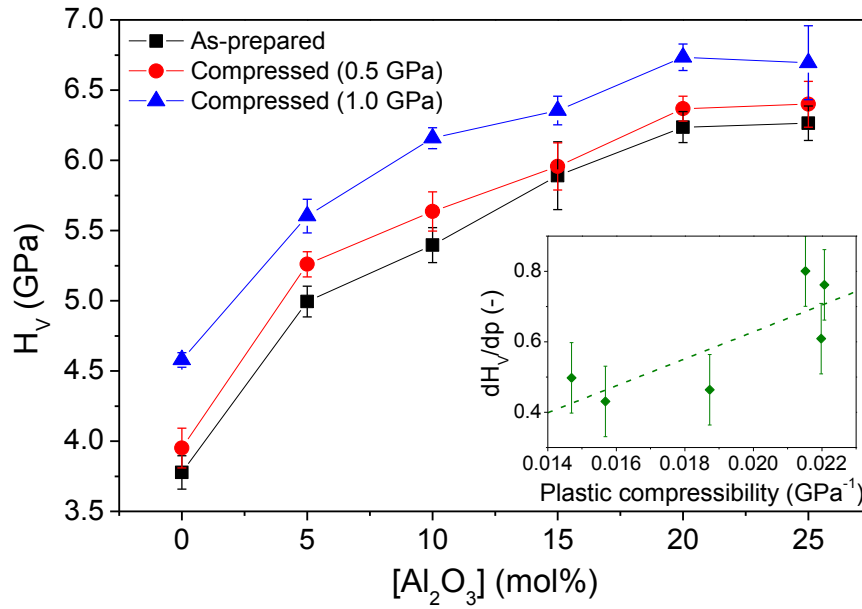
Figure 3. Crack resistance (CR) of the as-prepared and compressed sodium aluminosilicate glasses as a function of the Al_2O_3 content. CR is defined as the load causing 50% radial crack probability.
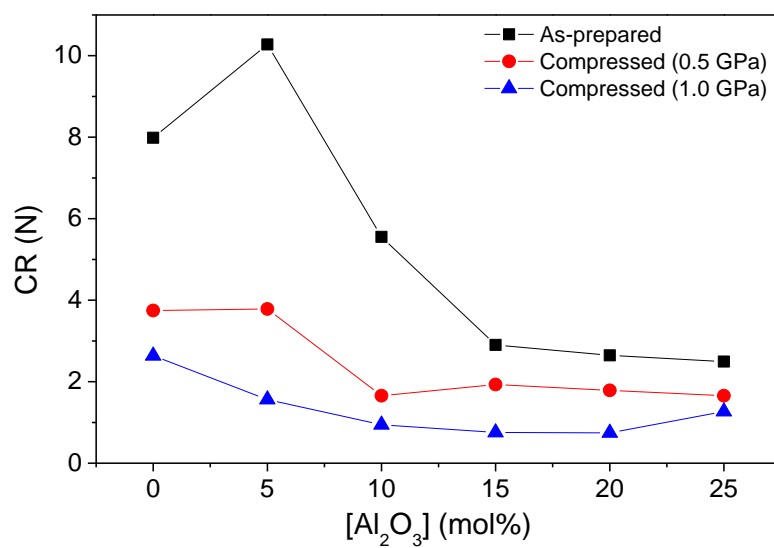
Figure 4. Raman spectra of the as-prepared sodium aluminosilicate glasses.
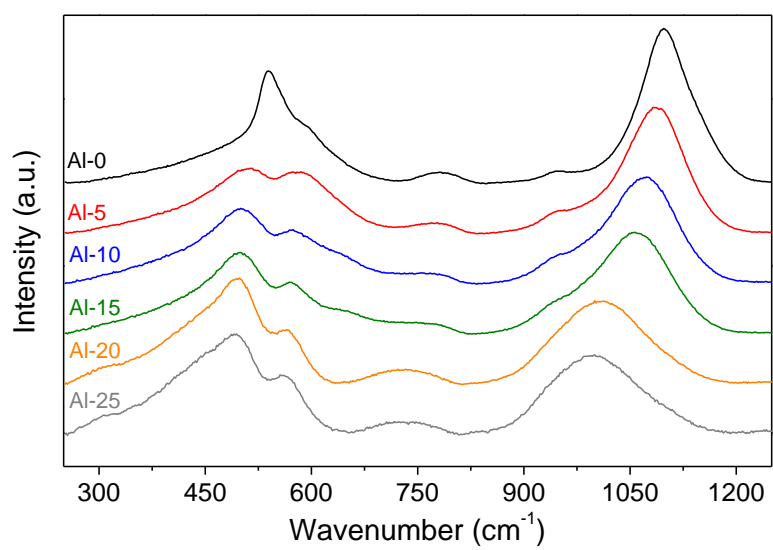
Figure 5. Peak positions of the Raman bands around 500 and 750 cm^{-1}, respectively, for the as-prepared sodium aluminosilicate glasses as a function of the Al_2O_3 content.
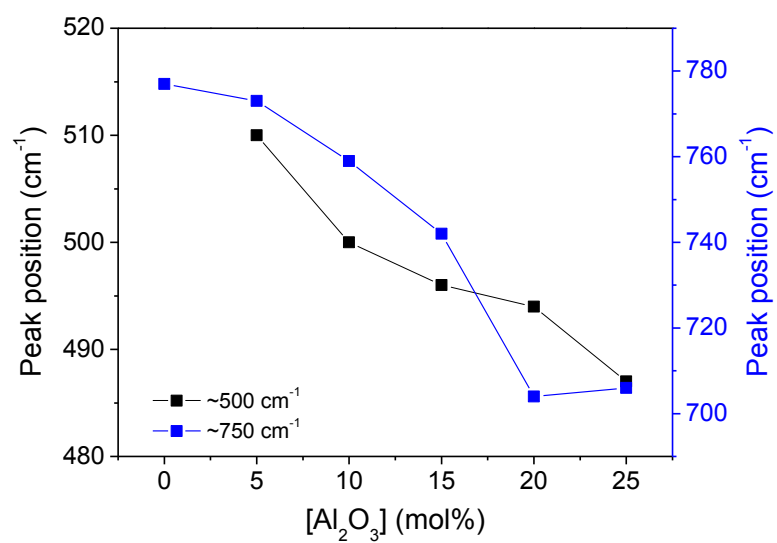
Figure 6. Deconvolution of the 850-1250 cm^{-1} frequency range of the Raman spectra for the as-prepared sodium aluminosilicate glasses. (a) Example of deconvolution for the as-prepared Al-10 glass. Peaks near 950, 1000, 1050, 1100, and 1125 cm^{-1} are due to vibrations of Q^2, Q^n, Q^3, $Q^{4,II}$, and $Q^{4,I}$, respectively (see the text for details). (b) Relative areas of these Raman bands for the as-prepared glasses as a function of the Al$_2$O$_3$ content.
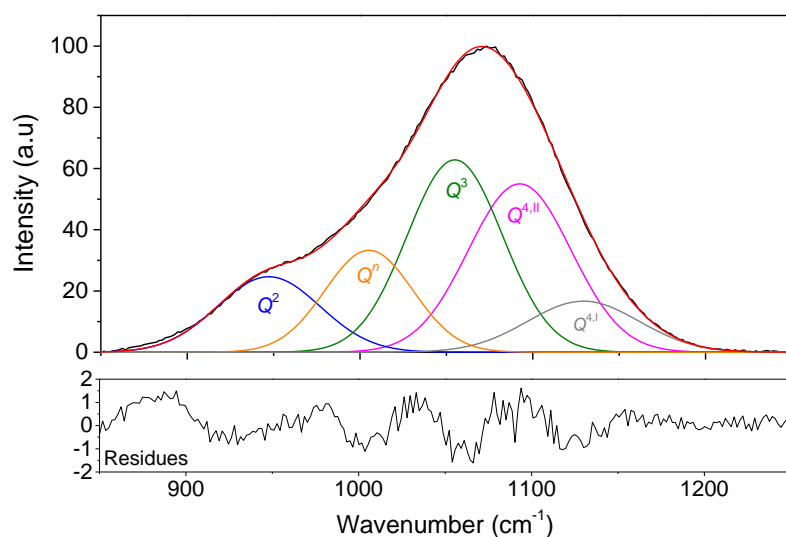
(a)
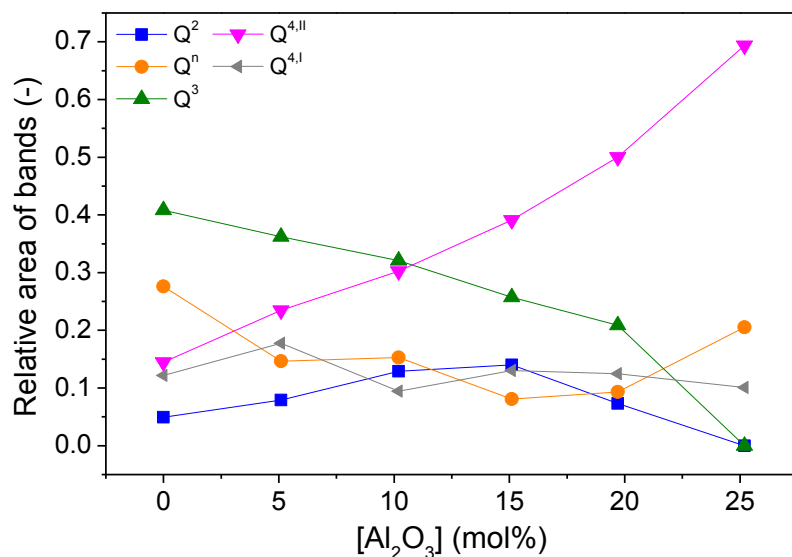
(b)

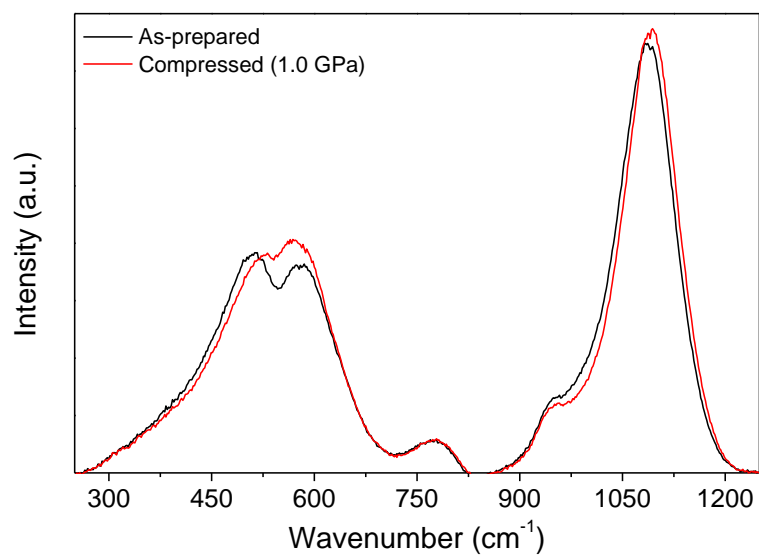**Figure 7.** Raman spectra of the as-prepared and compressed (at 1.0 GPa) Al-5 glass.

Figure 8. (a) ^{27}Al MAS NMR spectra for the five as-made glasses with compositions shown to the right of each spectrum. The inset shows an expanded view of the shift region for Al^V and Al^{VI} for three as-made glasses having a range of Al$_2$O$_3$ content. (b) ^{27}Al 3QMAS NMR spectrum for the as-made Al-5 glass. Contours are drawn to display Al^{IV} and Al^V peaks, as well as a very weak Al^{IV} spinning sideband to the top of the main peaks.
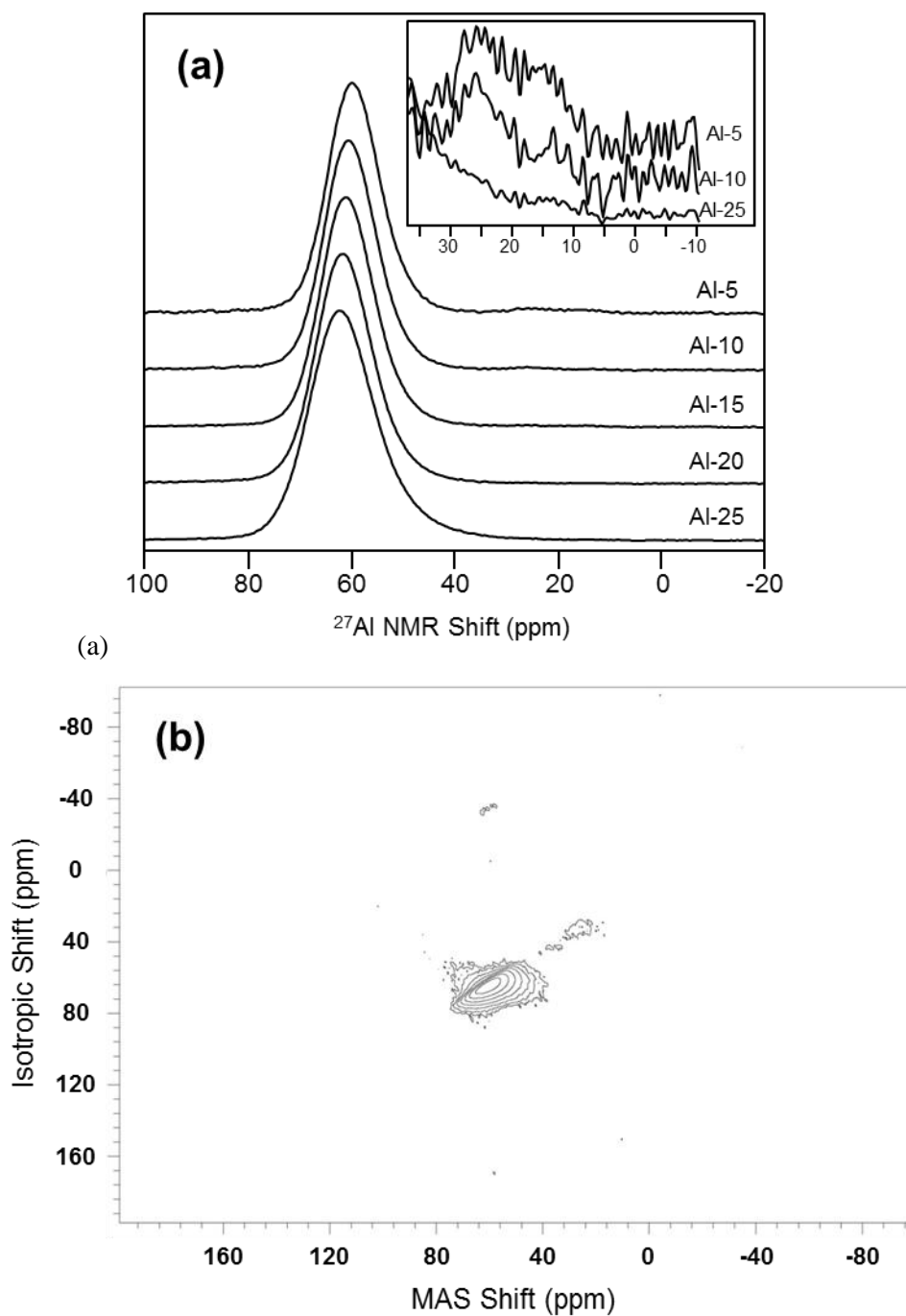

(a)

(b)

Figure 9. (a) ^{27}Al MAS NMR spectra for the five compressed (at 1.0 GPa) glasses with compositions shown to the right of each spectrum. (b) ^{27}Al 3QMAS NMR spectrum for the compressed Al-5 glass. Contours are drawn to display Al^{IV} and Al^{V} peaks, as well as a very weak Al^{IV} spinning sideband to the top of the main peaks.
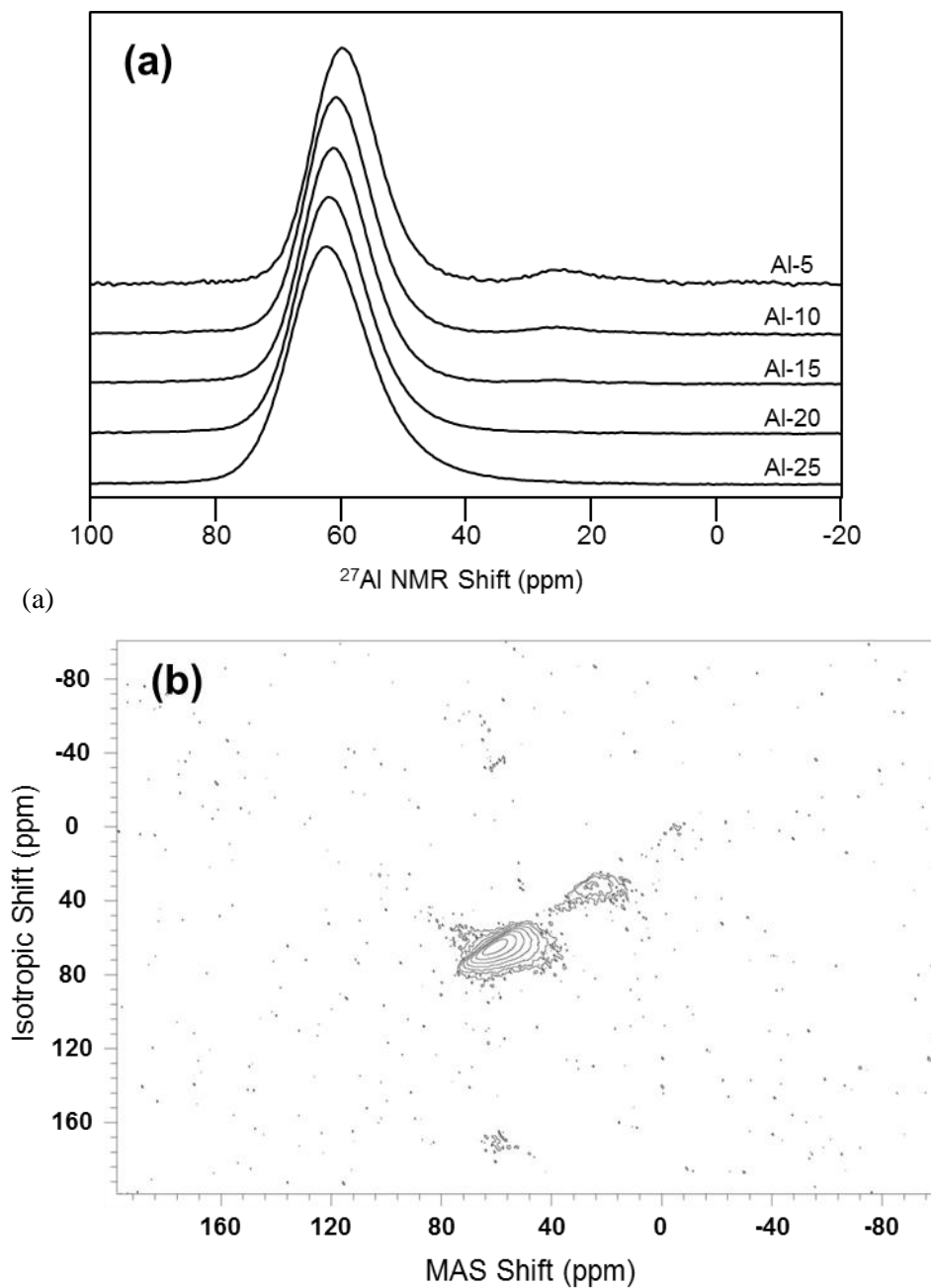

(a)

(b)

Figure 10. Isotropic projections from the ^{27}Al 3QMAS NMR spectra of (a) Al-5 glasses and (b) Al-10 glasses, where as-made glasses are shown in black and compressed glasses (at 1.0 GPa) are shown in gray. Al^{IV} and Al^{V} resonances are denoted.
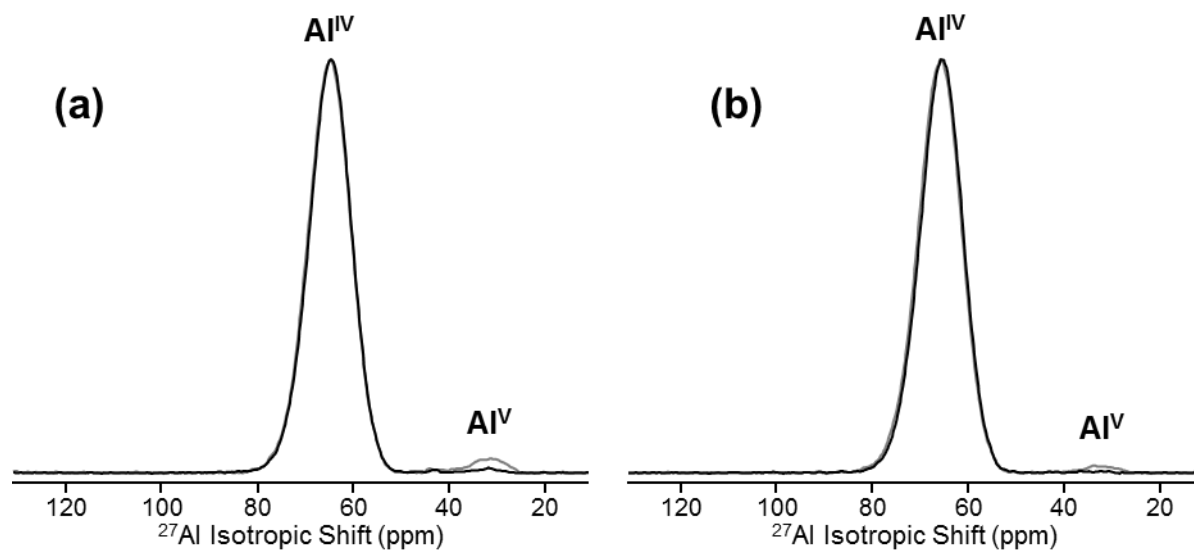
Figure 11. Fraction of five-fold coordinated aluminium (Al^V) as a function of the calculated number of non-bridging oxygens per tetrahedrally coordinated cation NBO/T for as-prepared and compressed (at 1.0 GPa) sodium aluminosilicate glasses.